Lattice Fluid Self-Consistent Field Theory of Surfaces with Anchored Chains

Douglas G. Peck and Keith P. Johnston*

Department of Chemical Engineering, The University of Texas, Austin, Texas 78712

Received July 6, 1992; Revised Manuscript Received December 7, 1992

ABSTRACT: Self-consistent field theory is combined with lattice fluid theory to produce a robust model of the structure and interactions of chains anchored to smooth surfaces. The inclusion of holes in the lattice provides a means to investigate the effects of bulk solvent density and temperature on the interfacial properties. In a good solvent at the incompressible limit, the interactions between the surfaces are repulsive but become attractive with the addition of free volume and compressibility, e.g. in alkane liquids. As density decreases, solvent is expelled from the higher density interfacial region to the lower density bulk phase. The solvent expulsion raises the entropy and increases the strength of the attractive interactions between the surfaces. This behavior is analogous to phase separation of bulk mixtures at the lower critical solution temperature. A novel result is that the forces between the surfaces become attractive at a much higher density than required for phase separation in bulk systems.

Introduction

The strength of interactions between surfaces modified with polymers is an important problem of theoretical and practical interest.[1] Practical applications include paint formulation, lubricant formulation, emulsion polymerization,[1] and both colloidal and microemulsion stability.[2-5] The effect of solvent/polymer/surface interactions must be understood to design optimal formulations for these applications. The available theoretical tools range from scaling theory[6] to random walk models,[7] self-consistent field theory,[8-12] integral equation theory,[13] and computer simulation.[14,15] Scaling theory is useful for qualitative predictions, especially for the influence of polymer chain length for long chains, but it is not highly quantitative. The random walk models are the easiest to use and require the least computer time. However, they do not consider interactions between chains explicitly or the influence of solvent size on the interfacial composition. Also, the segment density distribution is assumed to be independent of surface separation distance. Computer simulation has much promise, but many hours of computer time are required to treat all the interactions between the chains and solvent. The self-consistent field (SCF) theories are highly versatile because they account for all possible chain and solvent interactions and require orders of magnitude less computer time than full-scale computer simulation. The SCF theory provides a detailed representation both of the composition of the interfacial region and of the free energy of the system. This information is important for the understanding of the effect of polymer/solvent interactions on the interfacial thickness and the interaction strength between the surfaces.

The SCF theory has been applied to numerous systems. Initially, it was applied to the calculation of the structure and interaction of planar surfaces with adsorbed homopolymer.[9,10] In this case, the solvent was represented as a single segment. The theory was later modified to treat solvent molecules with more than one chain segment and to model the adsorption of block copolymers onto surfaces.[11] Analytical solutions have been obtained for certain cases, and a connection has been made between the Scheutjens and Fleer formalism and the self-consistent field continuum approach.[11d,e] It has also been applied to the calculation of the structure of bilayers, micelles, and vesicles for nonionic amphiphiles.[16-18] Recently, it has been modified to represent ionic components.[19] All of these models use an incompressible lattice, that is, the density throughout the interface is held constant. Recently, an SCF theory with a compressible lattice was developed for the study of homopolymers in contact with a vacuum.[20] We wish to explore this approach further, by deriving an SCF lattice fluid theory for a compressible lattice, for systems where a solvent is present in addition to polymer and holes.

Solvent density is an important property for the understanding of a variety of practical applications of colloidal and microemulsion systems. For example, in the formulation of lubricants, one must ensure that any colloidal particles present do not flocculate due to large temperature variations over which density can change significantly. Flocculation at high temperatures has been shown to be related to lower critical solution temperature phenomena.[21] For microemulsions stabilized in compressible solvents, density affects droplet size, droplet interactions, and the resulting phase behavior.[5] Even in systems not far from ambient temperature, it is possible that the density and compressibility can influence colloidal interactions and stability, although this issue has received little attention.

A key experimental apparatus for the study of interactions between surfaces is the force balance.[22] Usually, an amount of polymer is adsorbed from a solvent to the surface, and then the force vs distance profile is measured. A complicating feature of this approach is the variation in the amount of adsorbed polymer with distance.[22] That is, as the surfaces are forced together, polymer can be expelled from the surface. The resulting depletion layer can cause attractive forces.[10,13] However, polymer depletion would not be present for anchored chains. Another complication is the formation of polymer bridges between the surfaces.[1,21,22] The bridging can be eliminated to a large degree by adsorbing di- and triblock copolymers onto the surface.[22] Even for the block copolymers, the amount of adsorbed polymer can vary with distance. This problem has been addressed by grafting the polymer directly to the surface.[23]

Experimental studies indicate that surfaces with anchored chains exhibit repulsive interactions when the solvent is a "good" solvent, that is, for a Flory parameter $\chi \leq 1/2$ for long-chain polymers.[1] However, certain systems exhibit attractive interactions even when the solvent is good.[1] This behavior has been attributed to bridging of

0024-9297/93/2226-1537$04.00/0

the polymer between the surfaces. We will examine whether another phenomenon, the variation of the total density throughout the interfacial region, can also lead to attractive interactions.

It is well-known that density varies throughout an interfacial region and that this density gradient affects the interfacial free energy.[24] It would also be expected to influence the interaction energies of polymer-coated surfaces. In conventional mean field theories of bulk polymer solutions,[25] such as the Flory theory, the density is constant throughout the incompressible lattice. In the lattice fluid theory of Sanchez and Lacombe,[26] the presence of vacancies (holes) on the lattice allows for density variations; consequently, this theory can predict lower critical solution temperature phenomena. Our objective is to incorporate lattice fluid theory into SCF theories of interfaces to include the effects of compressibility. The density and composition in the interfacial region will be examined as a function of the bulk solvent density (concentration of holes). The interaction energy, entropy, and free energy will be analyzed in terms of the interfacial density and the extension of the chains. Additional important variables include the cohesive energy density of the solvent, the surface coverage of the chains, and the temperature. A detailed comparison of the SCF theory with and without compressibility is presented.

Theory

We will outline the development of the SCF theory[9,11] here so that the method of inclusion of compressibility will be clear. A general partition function of the system will be formulated to allow for multiple segment solvents. The surface is covered with anchored chains, component c, which are interpenetrated with solvent, component s. We allow density to vary by including holes, component o, in the lattice.

Self-Consistent Field Theory with an Incompressible Lattice. The grand canonical partition function can be written for this system as

$$\Xi(\{\mu_i\},M,L,T) = \sum_{\{n_i^d\}} Q(\{n_i^d\},M,L,T) \exp[\sum_i n_i\mu_i/kT] \quad (1)$$

where μ_i is the chemical potential of component i in the bulk, M is the number of lattice layers, L is the number of lattice sites per layer, Q is the canonical partition function, n_i^d is the number of molecules of type i in conformation d, and $n_i = \sum_d n_i^d$. The mean field approximation allows Q to be separated into combinatorial and energetic parts:

$$Q = \Omega \exp(-E/kT) \quad (2)$$

where Ω and E are the degeneracy and energy, respectively, of the system.

In the formalism of Scheutjens and Fleer, the degeneracy Ω of a collection of chains in contact with a surface is given by[9,11]

$$\ln(\Omega/\Omega^*) = \sum_{i,d} n_i^d \ln\left(\frac{L\lambda^d}{r_i n_i^d}\right) \quad (3)$$

where λ^d is a bond weighting factor for conformation d dependent on the lattice geometry, r_i is the number of segments in component i, and $\Omega^* = \prod_i \Omega^*_i$, where Ω^*_i is the degeneracy of the pure components. The expression for Ω^*_i is the well-known result from Flory.[11,25]

The expression for the mean field energy, E in eq 2, is obtained by counting the number of contacts between the various segments in the lattice. We use an approach similar to that of Scheutjens and Fleer, except the reference energy for the pure components E^* is written in terms of P^*_i the cohesive energy density (or characteristic pressure) of component i[27]

$$E^* = \sum_i v^* r_i n_i P^*_i \quad (4)$$

The characteristic pressure is a key physical property in lattice fluid theory. By employing the Bragg–Williams approximation, the energy for a lattice of M layers is

$$E = -Lv^* \sum_{z=1}^{M} \sum_i \sum_j \phi_i(z)\langle\phi_j(z)\rangle P^*_{ij} \quad (5)$$

The volume of layer z is Lv^*, and the average volume fraction of component j in layer z is $\langle\phi_j(z)\rangle = \lambda_1\phi_j(z-1) + \lambda_0\phi_j(z) + \lambda_1\phi_j(z+1)$. This equation can be factored[27] to yield

$$E = Lv^*kT\sum_{z=1}^{M}[\sum_i \sum_{j>i} \phi_i(z)\langle\phi_j(z)\rangle\chi_{ij} - \sum_i \phi_i(z)P^*_i/kT] \quad (6)$$

where $\chi_{ij} = [(P^*_i)^{1/2} - (P^*_j)^{1/2}]^2/kT$ if the geometric mean approximation is invoked, $P^*_{ij} = (P^*_i P^*_j)^{1/2}$. For a bulk system of pure components this equation reduces to eq 4.

At this point, the partition function of the system is defined. In order to find the equilibrium collection of chain conformations, the partition function must be maximized with respect to all of the possible chain conformations for a given concentration to yield[11]

$$\frac{\partial \ln Q}{\partial n_i^d} + \frac{\mu_i}{kT} - \sum_i \alpha(z) r_i^d(z) = 0 \quad (7)$$

where $r_i^d(z)$ is the number of segments of component i in conformation d and the Lagrange multiplier $\alpha(z)$ results from the constraint that each layer must be filled.[11]

Inclusion of Compressibility. The above equations, although with slightly different nomenclature, have been applied to systems composed of solvent and chains in the presence of surfaces.[9-11,28,29] In order to allow density to vary, we will introduce vacancies or holes into the lattice where each hole is only one segment long.[26,27] We begin with the first term in eq 7, which may be expressed as

$$\frac{\partial \ln Q}{\partial n_i^d} = \ln\frac{L\lambda^d}{r_i n_i^d} - 1 - \mu^*_i/kT - \frac{\partial(E-E^*)/kT}{\partial n_i^d} \quad (8)$$

The first three terms on the right-hand side result from the degeneracy. Because the holes occupy space in the same manner as the other components, these three terms are identical for compressible and incompressible lattices. The last term on the right-hand side of eq 8 is the energetic term. Because the interaction energy between a hole and any segment is by definition zero, the holes influence this term in a different manner than the other components.[27] As a result, the derivative of the energy term will be different for the lattice fluid and conventional SCF models. For the conventional SCF model,

$$(E-E^*) = Lv^*kT\sum_{z=1}^{M}\sum_i\sum_{j>i}\phi_i(z)\langle\phi_j(z)\rangle\chi_{ij} \quad (9)$$

For the lattice fluid SCF model,

$$(E - E^*) = Lv^*kT\sum_{z=1}^{M}[\sum_i\sum_{j>i} f_i(z)\langle f_j(z)\rangle\chi_{ij} - (1-\tilde{\rho}(z))\sum_i f_i(z)P^*_i/kT] \quad (10)$$

where $\tilde{\rho}(z) = V^*(z)/(Lv^*)$ is the reduced density of layer z, and $V^*(z)$ is the hard core volume of the layer (without the volume of the holes). The component volume fractions are represented as $f_i = r_in_i/(n_o + \sum_{i\neq o}r_in_i)$, where the subscript o represents the holes. In contrast, the hard core volume fraction, $\phi_i = r_in_i/\sum_{i\neq o}r_in_i$, is on a hole-free basis. When $\tilde{\rho} \to 1$, the system becomes incompressible, and eq 10 reduces to eq 9.

Equation 10 shows how the holes affect the internal energy.[27] As the number of holes increases, f_i decreases for the other components. This decreases the number of contacts between the segments. Thus, the addition of holes causes the internal energy to increase (become less negative).

The derivative of E may be expanded as[11]

$$\frac{\partial E}{\partial n_i^d} = \sum_z \frac{\partial E(z)}{\partial n_i(z)}\frac{\partial n_i(z)}{\partial n_i^d} \quad (11)$$

Evers has shown that $(\partial n_i(z)/\partial n_i^d) = r_i^d(z)$, where $r_i^d(z)$ is the number of segments of component i in conformation d in layer z.[11]

For the components that are not holes,

$$\frac{\partial E(z)}{\partial n_{i\neq o}(z)} = Lv^*[-(1-\tilde{\rho}(z))\sum_i f_i(z)P^*_i - \tilde{\rho}(z)P^*_i + kT\sum_j\langle f_j(z)\rangle\chi_{ij}] \quad (12a)$$

For the holes,

$$\frac{\partial E(z)}{\partial n_o(z)} = Lv^*\sum_i f_i(z)P^*_i \quad (12b)$$

Each of the above two equations can be combined with eq 8 to obtain the expression that can be solved for the concentration of components in a given conformation d

$$\ln\frac{L\lambda^d}{r_in_i^d} - 1 + (\mu_i - \mu^*_i)/kT + \frac{\partial E^*_i/kT}{\partial n_i} - \sum_{z=1}^{M} r_i^d(z)\left[\alpha(z) + \frac{\partial E/kT}{\partial n_i(z)} + u_i^{ref}\right] + \sum_{z=1}^{M} r_i^d(z)u_i^{ref} = 0 \quad (13)$$

where for convenience, a reference potential, u_i^{ref}, has been added and subtracted to the equation. The reference potential is selected so that the segment concentration approaches its bulk value far away from the interface. The closer the layer potential is to 0, the more the layer resembles the bulk.

Equation 14 could be solved for n_i^d at this point in the development, but the resulting equation would be unnecessarily complex. The following definitions, as made by Evers,[11] will make the final equation more tractable. First of all, the quantity in brackets is defined as $u_i(z)/kT$, which acts as a potential for segment i in layer z. An unnormalized "free segment weighting factor", $G_i(z)$, can be defined as a function of the segment potential

$$G_i(z) = \exp[-u_i(z)/kT] \quad (14)$$

in which the segment potentials are

$$u_{i\neq o}(z) = \alpha(z)kT - (1-\tilde{\rho}(z))\sum_k f_i(z)P^*_kv^* - \tilde{\rho}(z)P^*_iv^* + v^*kT\sum_j\langle f_j(z)\rangle\chi_{ij} + u_i^{ref} \quad (15a)$$

$$u_o(z) = \alpha(z)kT + v^*\tilde{\rho}(z)\sum_i f_i(z)P^*_i + u_o^{ref} \quad (15b)$$

Both of these expressions have the term $[\alpha(z) + v^*\tilde{\rho}(z)\sum_i f_i(z)P^*_i]$ in common, and this term is conveniently defined[11] as the hard-core potential, $u'(z)$, because it is the same for all components in each layer. After the reference potentials are determined by requiring that $u_i \to 0$ in the bulk, we then find that

$$u_{i\neq o}(z) = u'(z) - \sum_i[f_i(z) - f_i^b]P^*_iv^* - [\tilde{\rho}(z) - \tilde{\rho}^b]P^*_iv^* + v^*kT\sum_j[\langle f_j(z)\rangle - f_i^b]\chi_{ij} \quad (16a)$$

and

$$u_o(z) = u'(z) \quad (16b)$$

where f_i^b is the volume fraction of component i in the bulk. It is important to notice that the above equations reduce to the conventional SCF model results of Evers[11] when $\tilde{\rho} \to 1$, an important boundary condition.

Once the free segment weighting factors are known, the component volume fractions are calculated in the SCF formalism[9,11]

$$f_i(z) = C_i\sum_i G_i(z,s|1)G_i(z,s|r_i)/G_i(z) \quad (17)$$

where C_i is a normalization constant, and $G_i(z,s|1)$ is the chain weighting factor for segment s of chain i in layer z starting from the first segment. $G_i(z,s|1)$ is obtained through the recursion formula[9,11]

$$G_i(z,s|1) = G_i(z)\langle G_i(z-1,s|1)\rangle \quad (18)$$

where $\langle G_i(z,s|1)\rangle = \lambda_1G_i(z-1,s|1) + \lambda_oG_i(z,s|1) + \lambda_1G_i(z+1,s|1)$.

The normalization constant C_i could be calculated analytically,[11] but it is more convenient to calculate it numerically by invoking the bulk boundary conditions. For the components in equilibrium with the bulk, such as the solvent(s) and holes, $C_i = f_i^b/r_i$. In order to determine C_o, the bulk concentration of holes must be known. Because the lattice fluid SCF theory reduces to the Sanchez–Lacombe lattice fluid theory in the bulk, the lattice fluid theory can be invoked to calculate the value of $\tilde{\rho}^b$ at a given P and T for a particular solvent. Then $f_o^b = 1 - \tilde{\rho}^b$, and $f_i^b = \tilde{\rho}^b$ for the case of pure solvent.

The chains in this case are not in equilibrium with the bulk because they are anchored to the surface, so another technique is needed in order to calculate C_c. If the surface coverage of chains is specified in terms of $\theta_i = \sum_{z=1}^{M} f_i(z)$, the average number of chains per lattice layer, it can be shown[9,11] that

$$C_c = \theta_c/[r_c\sum_{z=1}^{M} G_c(z,r_c|1)] \quad (19)$$

The solution procedure is similar to that used by Scheutjens and co-workers except for a few differences. Given a T, P, and θ_c, the distribution of the components versus distance from the surface can be calculated using eq 17 as the basis. We start with an estimate of $u_i(z)$ for each component, $3M$ guesses. The free segment weighting

factors are calculated with eq 14. The normalization constant C_i is calculated for the solvent and holes from the Sanchez–Lacombe equation of state.[26,27] The other input value is θ_c, which is used to calculate C_c. The recursion formula, eq 18, is invoked in order to calculate the chain weighting factors that are used to calculate the component volume fractions with eq 17. Then, eq 16 is solved for $u'(z)$ for each component in every layer, $u'_i(z)$, and this solution is tested with the following $3M$ constraints. The first M constraints are the requirement that $\sum_i f_i(z) = 1$ for all layers. The other $2M$ constraints are that $u'_c(z) = u'_s(z)$ and $u'_s(z) = u'_o(z)$ for all layers. If the estimates for $u_i(z)$ do not satisfy these contraints, a new estimate of $\{u_i(z)\}$ is made with the Powell hybrid method available publicly as HYBRD from the MINPACK package (AT&T). We modified HYBRD slightly for this problem.[30]

Calculation of the Free Energy. Once the equilibrium distribution of components is know, another important interfacial property, the free energy of interaction between two surfaces with anchored chains, can be calculated. The Helmholtz free energy, A, is related to the canonical partition function as follows

$$A - A^* = -kT \ln(Q/Q^*) \tag{20}$$

Combining eqs 13, 14, 17, and 21, we obtain

$$(A - A^*)/kT = L\sum_i \frac{\theta_i}{r_i} \ln(r_i C_i) - \sum_{z=1}^{M}\sum_i f_i(z)u_i(z)/kT + \sum_{z=1}^{M} Lv^*\left[(1-\tilde{\rho}(z))\sum_i f_i(z)P^*_i/kT + \frac{1}{2}\sum_{i,j} f_i(z)\langle f_j(z)\rangle \chi_{ij}\right] \tag{21}$$

In order to calculate the free energy of interaction for a given surface separation distance M, we calculate at constant T, P, and $n_{i\neq o}$ the change in free energy between surfaces at a large separation distance M_∞, at which the chains do not ovelap, and at a separation distance M. When the surface separation distance decreases, the number of chains between the plates remains constant, but the number of solvent molecules decreases by $\Delta n_s(M)$. In order to keep the number of solvent molecules in the system constant, the same number of molecules is expelled into the bulk solvent. Then, the free energy of interaction $A(M)$ is

$$A(M) = (A - A^*)_M - (A - A^*)_{M\to\infty} + \Delta n_s(M)(\mu_s{}^b - \mu_s{}^*) \tag{22}$$

where $\mu_s{}^b$ and $\mu_s{}^*$ are the chemical potentials of the solvent in the bulk and reference state, respectively, and are calculated with the Sanchez–Lacombe equation of state.

The Gibbs free energy is given by $G = A + PV$, where P is the external pressure for the system, that is, the pressure in the bulk. Because the density in the interfacial region can differ from that in the bulk solvent, the volume of the system can change as solvent is expelled from the interfacial region to the bulk as the plates are brought closer together. Thus we write

$$G(M) = A(M) + P\Delta V(M) \tag{23}$$

where $\Delta V(M) = v^*L(M - M_\infty) + \Delta n_s(M)/\tilde{\rho}^b$ and is the change in volume of the system when the plates are brought from a surface separation distance of M_∞ to M.

Results and Discussion

Initially, we will compare the results from the lattice fluid SCF theory to previous results from the conventional SCF theory for a single surface with anchored chains in a single-segment solvent. After that section, all of the calculations will be made for two surfaces with anchored chains for a multisegment solvent, namely, pentane. The mechanism of the density effect on both the interfacial composition and the interaction energies between the two surfaces will be described in detail. Next, the influence of the parameters P^*_c and θ_c will be addressed. We will evaluate the ability of the conventional SCF theory to calculate the interfacial composition and interaction energy consistently for a single set of parameters. The consistency will be tested by comparing the results with the lattice fluid SCF model. Finally, temperature will be varied at constant pressure in order to calculate virial coefficients and flocculation temperatures for spherical surfaces.

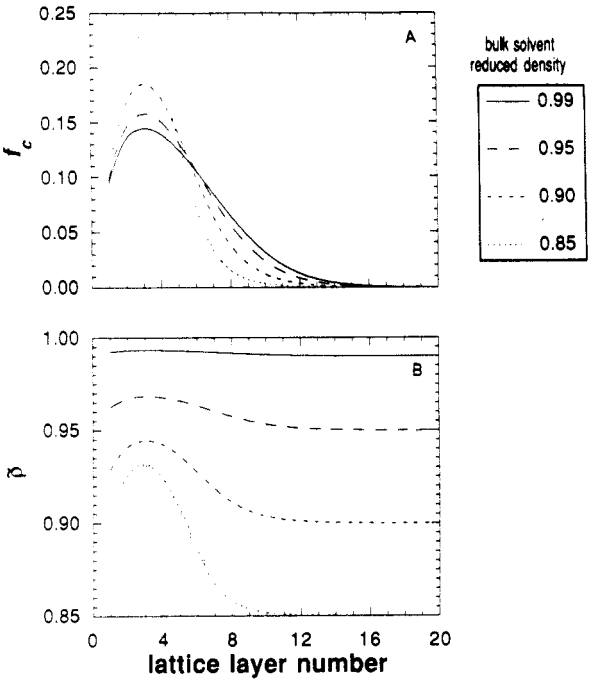

Figure 1. Effect of bulk solvent density on (A) the chain segment volume fraction profile and (B) the reduced density for chains anchored to a single surface. $r_c = 50$, $P^*_c = 7300$ atm, $r_s = 1$, $P_s^* = 3060$ atm, $\theta_c = 1.02$, $v^* = 11.82$ cm^3/mol, and $\chi = 0.6$.

Comparison with the Conventional SCF Theory. Figure 1A shows the chain segment volume fraction as a function of distance for the same system studied previously with the conventional SCF theory.[28] The range in $\tilde{\rho}^b$ includes densities of common hydrocarbon solvents often used in the study of polymer-coated surfaces. For example, the reduced density of these solvents ranges from 0.82 for butane to 0.89 for decane at ambient conditions. For the highest value of $\tilde{\rho}^b$, our model reduces to the conventional case as expected.[28] A profound density effect on the interfacial composition is observed as $\tilde{\rho}^b$ is decreased. The chains contract toward the surface, even though there is no adsorption energy for this system. At the incompressible limit, the root mean square end-to-end distance,[31] l_{rms}, is six lattice layers. Because the theory accounts for composition variations in the direction perpendicular to the surface only, l_{rms} is a measure of chain extension in this direction. On the basis of our calculations, the value of l_{rms} decreases by almost 50% when $\tilde{\rho}^b$ decreases from 0.99 to 0.80. Clearly, the interfacial thickness is a strong function of $\tilde{\rho}^b$. In contrast, interfacial thickness can be altered only through changes in χ in the conventional SCF theory.

Another novel aspect of this lattice fluid SCF theory is its ability to represent a variable density interfacial region,

Table I
Lattice Fluid SCF Parameters for the System Studied[a]

P^*_c = 4300 atm	v^* = 11.82 cm^3/mol
r_c = 50	T = 300 K
P^*_s = 3060 atm	θ_c = 3 (per surface)
r_s = 8	

[a] The solvent is pentane.

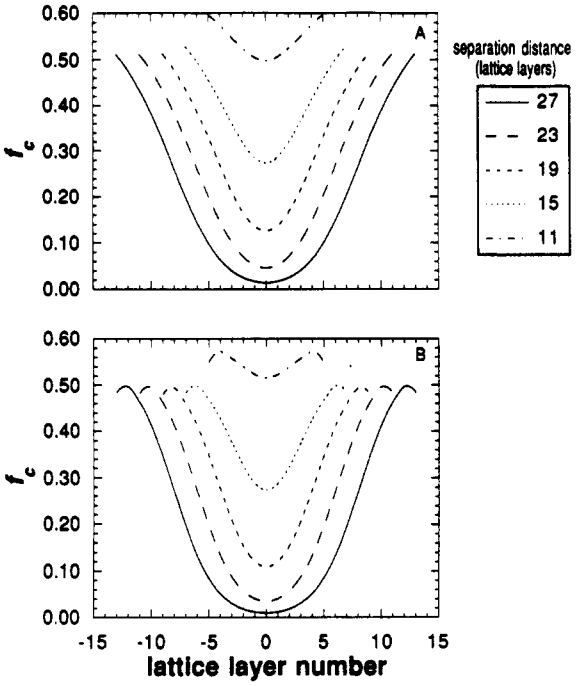

Figure 2. Chain segment volume fraction $f_i(z)$ at different plate separation distances: (A) $\tilde{\rho}^b$ = 0.99, (B) $\tilde{\rho}^b$ = 0.85. The center lattice layer is at zero. System parameters are in Table I.

as shown in Figure 1B. For the incompressible case where $\tilde{\rho}^b$ = 0.99, the density is constant. At lower bulk solvent densities, the reduced density becomes a strong function of distance from the surface. Far away from the surface, the reduced density equals the bulk solvent value but increases as the surface is approached. This disparity in reduced density between the interfacial and bulk regions increases as $\tilde{\rho}^b$ decreases, and it will have important consequences throughout this study.

Mechanism of the Density Effect. The mechanism of the density effect on both the interfacial composition and the interaction energy between the surfaces will be examined. The system we chose to study is represented by the parameters shown in Table I. The value of θ_c was chosen because it falls within the range of values studied in other applications of the incompressible SCF theory.[9,10,32] The Sanchez–Lacombe parameters, P^*, v^*, and r, for the solvent are those of a common hydrocarbon solvent, pentane. For a v^* of 11.82 cm^3/mol, the length of a cubic lattice site is 2.7 Å. The radius of gyration R_g is 3.1 sites or 8.5 Å. The Flory area is πR_g^2 or 226 Å^2. The grafted area per chain, which is calculated from r and θ_c, is equal to (7.3 Å^2/site) (50 segments/chain)/(3 segments/surface site) = 121 Å^2/chain. Therefore, these conditions represent a brush state.

In Figure 2A,B, the chain segment distributions at selected plate separation distances are shown for the incompressible case, $\tilde{\rho}^b$ = 0.99, and also for $\tilde{\rho}^b$ = 0.85, respectively. If the chains were completely extended, f_c would be constant at 0.06. For both values of $\tilde{\rho}^b$ shown in the figures, $f_c(z)$ near the surface is considerably larger than 0.06, indicating that the chains have contracted toward the surface. In both figures, the chains attached

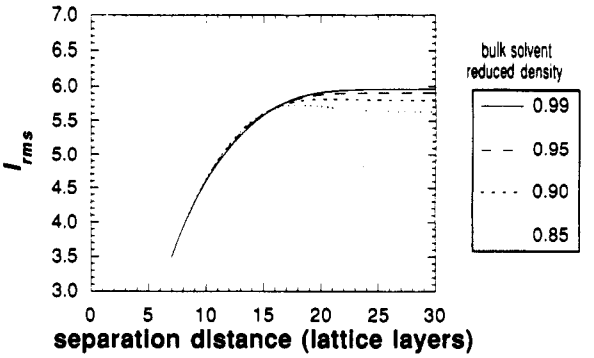

Figure 3. Chain l_{rms} as a function of plate separation distance at different values of $\tilde{\rho}^b$. System parameters are in Table I.

to both surfaces begin to overlap at a surface separation distance of 27 lattice layers, slightly more than half the completely extended chain length. As the surfaces are brought closer together, the chains overlap markedly, as indicated by the large increase in f_c at the lattice layer equidistant from each surface. When the surfaces are 11 lattice layers apart, the chains are highly compressed against the surfaces, as indicated by the large value of f_c over the entire region between the surfaces.

The forms of the chain segment distributions are different for the two values of $\tilde{\rho}^b$. At the incompressible limit, $f_c(z)$ is maximum in the lattice layer adjacent to the surface. In contrast, a lower value of $\tilde{\rho}^b$ = 0.85 causes a maximum in $f_c(z)$ to occur a few layers away from each surface. Even though this difference is small, it does indicate that the character of the chain segment distribution can change with $\tilde{\rho}^b$.

In Figure 3, the l_{rms} is shown as a function of distance over a range of $\tilde{\rho}^b$. At large surface separation distances where the chains attached to each surface do not overlap, l_{rms} decreases with decreasing $\tilde{\rho}^b$. For all values of $\tilde{\rho}^b$, the value of l_{rms} decreases with a decrease in surface separation distance because of the restriction imposed on the chains by the impenetrable surfaces. Where the surface separation distance is less than 15 lattice layers, l_{rms} is insensitive to $\tilde{\rho}^b$. Here, the chains are highly compressed against the surface, as was seen above in Figure 2A,B. For a separation distance of 11 lattice layers, the interfacial density is invariant over most of the space between the surfaces at each value of $\tilde{\rho}^b$, 0.85–0.99 (Figure 4A). Here, the effect of $\tilde{\rho}^b$ on the chain segment distribution is small, Figure 3. In contrast, the same change in $\tilde{\rho}^b$ produces a pronounced effect on the form of the $\tilde{\rho}$ curve when the separation distance is larger (Figure 4B). Here, the chain segment distribution is sensitive to changes in $\tilde{\rho}^b$.

The reduced density of the layers closer to the surface is greater than the bulk solvent-reduced density (Figure 4B), as was also the case in Figure 1B. This density gradient is important because it leads to a change in volume as the surfaces are brought together, as shown in Figure 5, even though the amounts of solvent and polymer are held constant. In all cases, the volume expands as solvent is expelled from the higher density interfacial region to the lower density bulk region. With the conventional SCF theory, this behavior cannot be represented. In bulk solution thermodynamics, large changes in volume on mixing are important because they can lead to phase separation at the lower critical solution temperature (LCST). By analogy, these volume changes are expected to influence interaction free energies between surfaces.

In Figure 6A, the Gibbs free energy of interaction for two surfaces vs surface separation distance is shown. The value of $G(M)$ is zero at the reference, infinite separation

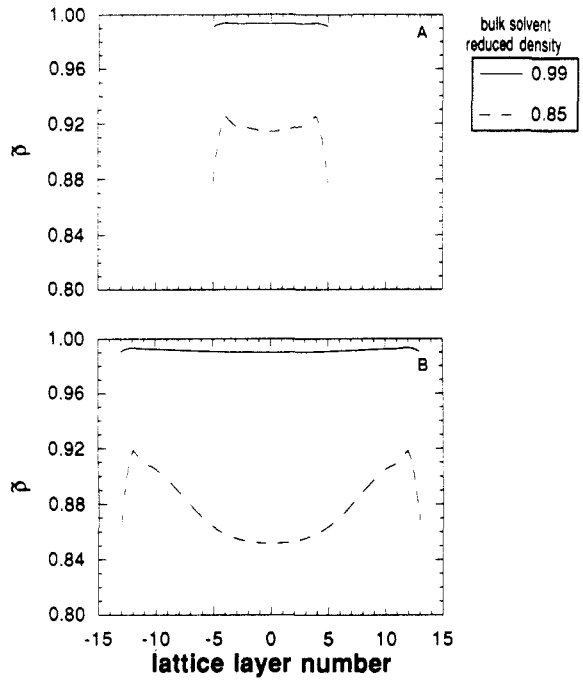

Figure 4. Effect of solvent-reduced density on $\tilde{\rho}(z)$ at a separation distance of (A) 11 and (B) 27 lattice layers. System parameters are in Table I.

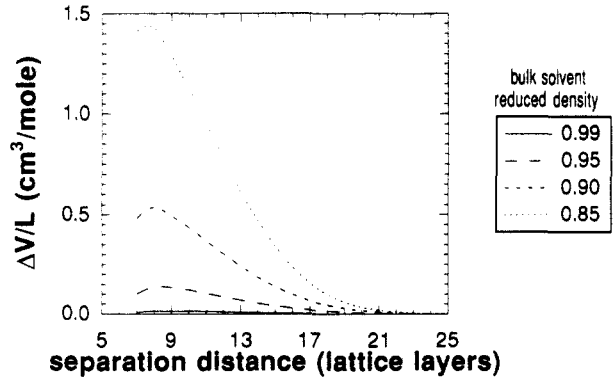

Figure 5. $\Delta V/L$ (cm³/mol) vs separation distance at different values of $\tilde{\rho}^b$ for the system parameters in Table I.

distance. Notice that the bulk solvent density has a pronounced effect on the interaction energy. At the incompressible limit ($\tilde{\rho}^b = 0.99$), the interactions are repulsive, but as $\tilde{\rho}^b$ decreases, the interaction energy becomes attractive. This is the first time this continuous transition from repulsive to attractive interactions has been predicted as a function of bulk solvent density.

A bulk solution of pentane and chains with the parameters shown in Table I would have an LCST of 414 K. In the terminology of Napper,[1] the solvent would be a "good" solvent, and repulsive interactions would be expected. In contrast, attractive interactions are observed. Previous investigators have reported attractive interactions for surfaces coated with polymer in a "good" solvent, but the interactions were attributed to bridging of the polymers between the surfaces. In our model, there is no adsorption energy for the chains onto the surface, so bridging is not present. Thus, this demonstrates that another mechanism, variation in the bulk solvent density, can lead to attraction between the surfaces.

In order to understand the role of solvent density on the interaction free energy, we examine both the internal energy and entropy of interaction. The calculations were performed over one K temperature increments in order to determine the internal energy and entropy components

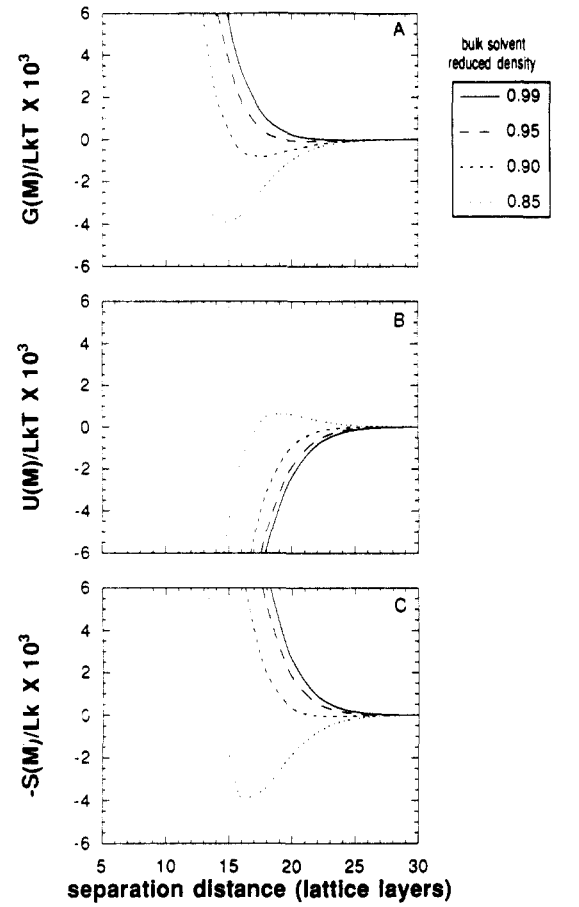

Figure 6. (A) Gibbs free energy of interaction between two flat surfaces with anchored chains vs separation distance at various values of $\tilde{\rho}^b$. System parameters are in Table I. (B) Internal energy of interaction. (C) Entropy of interaction.

of $G(M)$. The entropic component is given by

$$S(M) = -(\partial G(M)/\partial T)_P \tag{24}$$

and the internal energy component is given by

$$U(M) = G(M) - TS(M) - P\Delta V(M) \tag{25}$$

The internal energy of interaction is illustrated as a function of surface separation distance and density in Figure 6B. As the surfaces are brought together at a given solvent-reduced density, the chains overlap, and solvent and holes are expelled. This decreases the number of chain/solvent contacts and causes $U(M)$ to become more negative because $\chi > 0$. At a given separation distance, a decrease in $\tilde{\rho}^b$ increases the number of holes between the surfaces. Consequently, the number of segment contacts decreases, the $U(M)$ becomes less negative.

The entropy of interaction, shown in Figure 6C, has the same form as the free energy of interaction. This similarity indicates that entropy appears to determine the form of the free energy curve. At the higher values of $\tilde{\rho}^b$, the entropic contribution of $G(M)$ is repulsive; that is, the entropy decreases as the surfaces are brought together. This is due to the entropic restriction imposed on the chains by the surfaces, as the chains are compacted into a small volume. For lower values of $\tilde{\rho}^b$, the character of the entropic contribution curve changes. At the onset of chain overlap, the entropic contribution is attractive; that is, the entropy increases. This favorable condition is due to the expansion of solvent from the higher density interfacial region to the lower density bulk solvent, as shown in Figure 5.

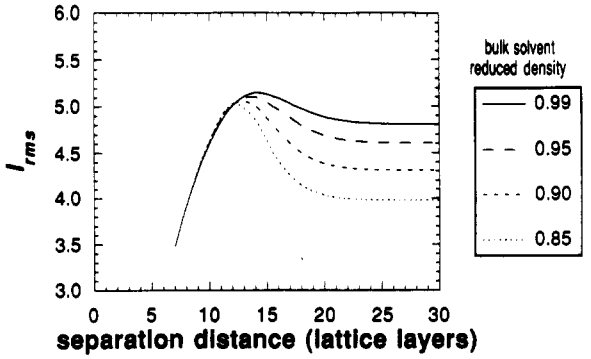

Figure 7. Chain l_{rms} as a function of plate separation distance at different values of $\tilde{\rho}^b$. System parameters are in Table I, except P^*_c = 5000 atm.

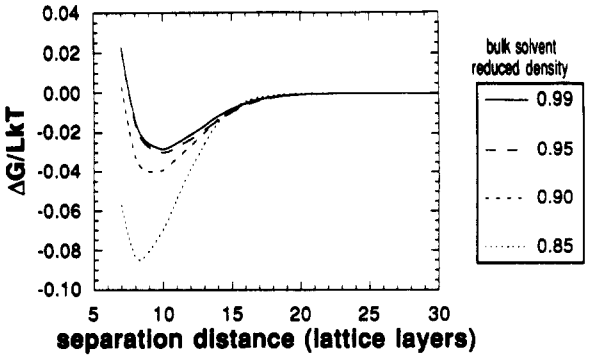

Figure 8. Gibbs free energy of interaction vs separation distance at various values of $\tilde{\rho}^b$. System parameters are in Table I, except P^*_c = 5000 atm.

This entropy-driven attraction between surfaces is analogous to phase separation at a lower critical solution temperature (LCST) in bulk polymer solution. In each case, solvent molecules are demixed from the polymer chains to increase the system entropy by increasing the total volume. In the case of interacting surfaces, these attractive entropic interactions could cause flocculation.[1] Typically, the LCST in bulk solution occurs as the density is reduced to $\tilde{\rho}^b \sim 0.5$. However for interfacial systems, the interaction free energy can change from repulsive to attractive at much higher values of $\tilde{\rho}^b$, e.g. 0.9 in Figure 6A. Thus, interactions between surfaces can be more sensitive to density than those in bulk polymer solutions, because of the reduced density gradient in the interface.

When two surfaces are brought very close to each other, the interaction becomes repulsive (Figure 6A). Even though the change in the total system volume remains positive, the entropic interaction becomes repulsive. Here, the entropy decreases because of the restricted volume for the highly compressed chains between the surfaces.

Another effect of bulk solvent density is on the location of the repulsive wall in the free energy of interaction. At lower densities the chains contract toward the surface, thus the repulsive wall in the interaction free energy shifts to smaller separation distances, as shown in Figure 6B.

Influence of P^*_c. Another important parameter in the theory is P^*_c, a constant that represents the energy density of chains at their closest-packed density ($\tilde{\rho}$ = 1). When holes are added, the cohesive energy density of the mixture of chains and holes decreases. In this study, P^*_c is always greater than P_s^*. Therefore, an increase in P^*_c increases χ, eq 6. An increase in χ causes the chains to contract toward the surface because of the reduction in solvent quality.[10,11] For the lattice fluid SCF theory for a given $\tilde{\rho}^b$, increasing P^*_c causes the chains to pack against the surface, as indicated by the decrease in l_{rms} at a given $\tilde{\rho}^b$ as observed by comparing Figures 3 and 7. At $\tilde{\rho}^b$ = 0.8, a change in P^*_c from 4300 to 5000 atm decreases l_{rms} from 5.6 to 4.0 lattice layers at M = 30. Mechanistically, an increase in P^*_c causes the energetic chain/chain interactions to become favored relative to chain/solvent interactions. As a result, solvent and holes are expelled from the interfacial region, and the chains become more compacted against the surface.

The increase of P^*_c also changes the characteristic behavior of the l_{rms} vs distance curve. When P^*_c = 5000 atm, the l_{rms} curve goes through a maximum for all of the values of $\tilde{\rho}^b$. As the surfaces are brought together, the chains begin to overlap and extend in order to increase the number of chain/chain contacts, causing l_{rms} to increase. At smaller separation distances, the volume restriction of the surfaces on the chains forces the chains to contract, causing l_{rms} to go through a maximum and then to decrease. In order for the chains to extend, solvent must be expelled. This behavior is not present when P^*_c was 4300 atm (Figure 3). When P^*_c is increased from 4300 to 5000 atm, the chain/chain interactions become sufficiently favorable that chain extension occurs. This effect becomes more pronounced as $\tilde{\rho}^b$ decreases because of the poorer solvation of the chains.

We also observed at a given value of $\tilde{\rho}^b$, an increase in P^*_c causes an increase in the reduced density near the interface. Thus, the difference between the interfacial and bulk densities increases as P^*_c increases.

Even though the effect of P^*_c on the interfacial composition is moderate, its effect on the interaction energy is large, as shown in Figure 8 compared with Figure 6A. At all of the values of $\tilde{\rho}^b$, the free energy of interaction is more attractive than the case with P^*_c = 4300 atm. The larger value of P^*_c enhances the energetic interaction of the chains between the two surfaces. Also, because the density difference between the interfacial and bulk regions increases with P^*_c, the entropic attraction becomes stronger. Thus, the free energy of interaction is more sensitive to $\tilde{\rho}^b$ when P^*_c is larger.

The results of this section can shed light on an interesting experimental observation, that is hysteresis in the force vs distance profile for polystyrene chains adsorbed onto mica surfaces in a mixture of toluene and heptane.[33] When the surfaces were being separated, the forces were attractive, but when the surfaces were brought together, the interactions were repulsive. On the basis of our results for the case with P^*_c = 5000 atm, the chains prefer to extend as the surfaces are brought together. If the relaxation time of the chains were low compared to the time scale of force balance measurements, one may expect kinetics to affect experimental results. This hysteresis has been attributed to adhesion of the chains to the surfaces by the formation of bridges,[33a] but even if bridging is not present, our results indicate that the chain reorientation could cause this hysteresis.

Influence of θ_c. Another important parameter is the amount of polymer on the surface. When θ_c increases from 3 to 5 while all other parameters in Table I are kept constant, l_{rms} increases from 5.6 to 6.6 lattice layers at surface separation distances where no chain overlap occurs. On a given surface, the higher coverage forces the chains outward modestly. The effect of the increase in interfacial thickness causes the interaction free energy curve to shift toward larger separation distances while the depth of the attractive well changes slightly. This behavior agrees with results from the conventional SCF theory.[11]

Consistency. In this section, we examine the ability of the conventional SCF model to reproduce our results

Table II
Effective χ for the Conventional SCF Model Regressed from the Chain Volume Fraction Profile for the Lattice Fluid SCF Model

$\tilde{\rho}$ for lattice fluid SCF model	effective χ
0.85	0.0769
0.80	0.0860

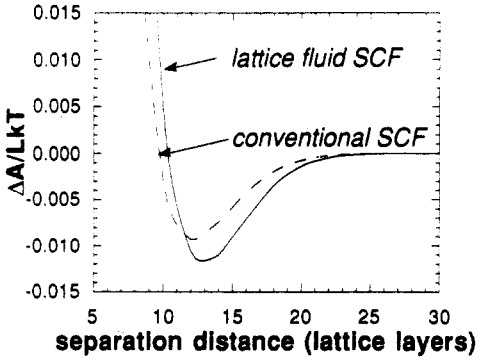

Figure 9. Comparison between the conventional and the lattice fluid SCF theories for the Helmholtz free energy of interaction ($\tilde{\rho}^b = 0.80$).

obtained with the lattice fluid SCF model. The question is, can the conventional SCF model give consistent results for both the interfacial composition and the interaction free energy with a single set of parameters. Again, we consider the system defined in Table I. For the conventional SCF model, χ was varied until the resulting chain volume fraction profile was most similar to the profile produced with the lattice fluid SCF theory at a give value of $\tilde{\rho}^b$. The sum of the squares of the difference between the volume fraction profiles was minimized. The values obtained are in Table II. Once this effective χ was determined, it was used to calculate the interaction free energy. When $\tilde{\rho}^b = 0.85$, the interaction energy curves for the two models are similar, but not exactly the same. When $\tilde{\rho}^b = 0.80$, the free energies differ significantly, as shown in Figure 9. In addition, χ (conventional model) is no longer constant but becomes an effective χ which is a function of solvent bulk density because the solubility parameter of the solvent varies with density. For the conventional SCF model, χ only affects the internal energy. However, the holes affect the free energy both through the internal energy and entropy. Thus, the effective χ must account for the effect of solvent density on both the internal energy and the entropic contributions to the interaction energy. Clearly, the new lattice fluid SCF theory predicts the effect of solvent density on both the interfacial composition and the interaction free energy of the surface much more effectively than the conventional SCF theory.

Effect of Temperature. Up to this point, we have examined changes in density at constant temperature. Colloidal systems composed of spheres coated with polymer have been identified that exhibit flocculation when the temperature increases,[1,21] but attempts to model these data have been limited. The flocculation temperature has been correlated roughly to the lower critical solution temperature (LCST) of a mixture of the polymer and solvent by using effective χ parameters. However, this approach does not provide quantitative information about the variation in the interaction strength or the interfacial structure of the interface with temperature. With the lattice fluid SCF theory, this information can be predicted.

The interaction free energy curve can be predicted as a function of temperature at a constant pressure, as shown in Figure 10. The depth of the attractive well increases

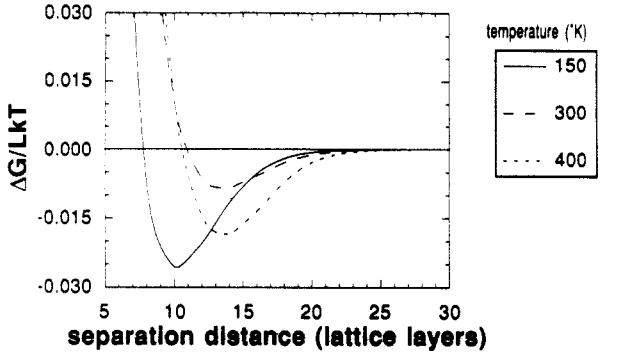

Figure 10. Effect of T on the Gibbs free energy of interaction. System parameters are in Table I, P = 15 bar.

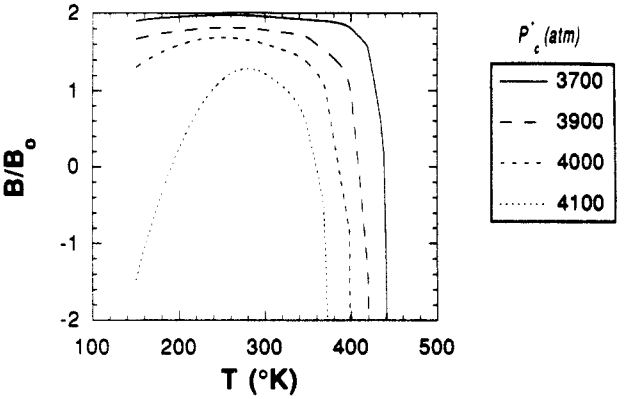

Figure 11. Second virial coefficient vs T for several values of P^*_c. B_0 is the value for hard spheres, $2/3\pi d^3$. The sphere diameter is 20 nm. System paramters are in Table I.

Table III
$T_{B=0}$ for Different Values of P^*_c Compared with the LCST for a Bulk System

P^*_c (atm)	$T_{B=0}$ (K)	LCST (K)
4100	360	444
4000	385	450
3900	410	454
3700	435	455

as T changes from 300 to 150 K. As T decreases the solvent density increases slightly and has little effect, but the value of χ increases, as shown in eq 6. This change causes the internal energy of interaction to become more favorable as solvent is expelled from the interfacial regions as the surfaces are brought together. As a result, the attractive interactions become stronger. Thus, the increase in the strength of attractive interactions as T decreases is enthalpically driven, just as with phase separation at the upper critical solution temperature in bulk polymer/solvent mixtures.[28]

The novel aspect of these results is that the depth of the attractive well also increases as T increases from 300 to 450 K. At the higher temperatures, increasing T decreases χ, but $\tilde{\rho}^b$ decreases significantly. The effect of $\tilde{\rho}^b$ dominates and leads to entropically driven attraction as discussed above.

The information in each $G(M)$ curve can be integrated using the Derjaguin approximation[34] to obtain a potential vs distance curve for two spheres with a given radius. This potential can be integrated to obtain a second virial coefficient, as shown in Figure 11 for various values of P^*_c. The temperature at which B becomes zero, $T_{B=0}$, is the point where the spheres are attracted to each other (see Table III). For comparison, the LCST for the bulk polymer/solvent system, as calculated from the Sanchez–Lacombe equation of state,[28] is shown. As expected from

previous experimental observations,[1,21] $T_{B=0}$ is well above ambient temperature and approaches the LCST. In fact, when P^*_c decreases toward P_s^*, the difference between $T_{B=0}$ and the LCST decreases. The system behaves more like a bulk system because, as shown above, the difference between the interfacial and bulk densities decreases. In contrast, when the difference between P^*_c and P_s^* becomes larger, the difference between the interfacial and bulk densities becomes larger. This density difference makes the attraction stronger because of the entropy associated with solvent expulsion. Consequently, $T_{B=0}$ becomes significantly less than the LCST. Here, the onset of attractive interactions occurs at much higher values of $\tilde{\rho}^b$ than those encountered at the LCST.

Conclusions

The lattice fluid self-consistent field theory offers a means to predict both the composition and interactions of surfaces with anchored chains as a function of bulk solvent density. At the incompressible limit ($\tilde{\rho}^b = 0.99$) the model reduces to the conventional SCF theory. As $\tilde{\rho}^b$ is reduced, the solvent increases its entropy by migrating from the higher density interfacial region to the bulk. Consequently, the difference between the interfacial and bulk densities increases and the chains contract toward the surface. In addition, the entropy of interaction between the surfaces becomes more favorable because of the solvent expulsion from the interfacial region. This causes the free energy of interaction to become attractive. This phenomenon is analogous to the occurrence of the lower critical solution temperature (LCST) in bulk solutions. A novel result is that the forces between the surfaces become attractive at a much higher density than required for phase separation in bulk systems.

With the lattice fluid SCF model, the influence of temperature on colloidal interactions is understood at a microscopic level. The temperature at which the interactions become attractive, $T_{B=0}$, is somewhat lower than the bulk lower critical solution temperature (LCST). As the chain/solvent interactions become more unfavorable (χ increases), the difference between $T_{B=0}$ and the LCST increases because of the greater degree of density variation throughout the interface. Without the inclusion of holes, this phenomenon could not have been predicted.

Acknowledgment. This work was supported by the National Science Foundation under Grant No. CTS-8900819. Any options, findings, and conclusions or recommendations expressed in this publication do not necessarily reflect the views of the National Science Foundation. Further support was provided by the State of Texas Energy Research in Applications Program, the Camille and Henry Dreyfus Foundation for a Teacher-Scholar Grant (to K.P.J.), the Separations Research Program, and the Center for Energy Studies at the University of Texas. We thank Patricia Hurter for providing us with test cases for the conventional SCF theory. We acknowledge helpful discussions with Isaac Sanchez, M. Muthukumar, Alice Gast, and Sanat Kumar.

References and Notes

(1) Napper, D. H. *Polymeric Stabilization of Colloidal Dispersions*; Academic Press: London, 1983.
(2) Ruckenstein, E.; Rao, I. V. *Colloids Surf.* **1986**, *17*, 185.
(3) Lemaire, B.; Bothorel, P.; Roux, D. *J. Phys. Chem.* **1983**, *87*, 1023. Roux, D.; Bellocq, A. M.; Bothorel, P. In *Surfactants in Solution*; Mittal, K. L., Lindman, B., Eds.; Plenum: New York, 1984; Vol. 3, p 1843.
(4) Kaler, E. W.; Billman, J. F.; Fulton, J.; Smith, R. D. *J. Phys. Chem.* **1991**, *95*, 458.
(5) Peck, D. G.; Schechter, R. S.; Johnston, K. P. *J. Phys. Chem.* **1991**, *95*, 9541. Peck, D. G.; Johnston, K. P. *J. Phys. Chem.* **1991**, *95*, 9549.
(6) Alexander, S. *J. Phys. (Paris)* **1977**, *38*, 983. de Gennes, P.-G. *Macromolecules* **1980**, *13*, 1069.
(7) Meier, D. J. *J. Phys. Chem.* **1967**, *71*, 1861. Hesselink, F. Th. *J. Phys. Chem.* **1969**, *73*, 3488.
(8) Dolan, A. K.; Edwards, S. F. *Proc. R. Soc. London, A* **1975**, *343*, 427.
(9) Schuetjens, J. M. H. M.; Fleer, G. J. *J. Phys. Chem.* **1979**, *83*, 1619. Scheutjens, J. M. H. M.; Fleer, G. J. *J. Phys. Chem.* **1980**, *84*, 178.
(10) Scheutjens, J. M. H. M.; Fleer, G. J. *Macromolecules* **1985**, *18*, 1882.
(11) (a) Evers, O. A.; Scheutjens, J. M. H. M.; Fleer, G. J. *Macromolecules* **1990**, *23*, 5221. (b) Evers, O. A.; Scheutjens, J. M. H. M.; Fleer, G. J. *J. Chem. Soc., Faraday Trans.* **1990**, *86*, 1333. (c) Evers, O. A.; Scheutjens, J. M. H. M.; Fleer, G. J. *Macromolecules* **1991**, *24*, 5558. (d) Semenov, A. N. *Sov. Phys.—JETP (Engl. Transl.)* **1985**, *61*, 733. (e) Milner, S. T.; Witten, T. A.; Cates, M. E. *Macromolecules* **1988**, *21*, 2610.
(12) Muthukumar, M.; Ho, J.-S. *Macromolecules* **1989**, *22*, 965.
(13) Yethiraj, A.; Hall, C. K. *J. Chem. Phys.* **1991**, *95*, 3749. Yethiraj, A.; Hall, C. K. *J. Colloid Interface Sci* **1992**, *151*, 102.
(14) Murat, M.; Grest, G. S. *Macromolecules* **1989**, *22*, 4054. Murat, M.; Grest, G. S. In *Computer Simulation of Polymers*; Roe, R. J., Ed.; Prentice Hall: Englewood Cliffs, NJ, 1991; p 141.
(15) Kumar, S. K.; Szleifer, I.; Panagiotopoulos, A. Z. *Phys. Rev. Lett.* **1991**, *66*, 2935.
(16) Leermakers, F. A. M.; Scheutjens, J. M. H. M.; Lyklema, J. *Biophys. Chem.* **1983**, *18*, 353. Leermakers, F. A. M.; Scheutjens, J. M. H. M. *J. Chem. Phys.* **1988**, *89*, 3264. Leermakers, F. A. M.; Scheutjens, J. M. H. M. *J. Phys. Chem.* **1989**, *93*, 7417. Leermakers, F. A. M.; Scheutjens, J. M. H. M. *J. Colloid Interface Sci.* **1990**, *136*, 231.
(17) Cogan, K. A.; Leermakers, F. A. M.; Gast, A. P. *Langmuir* **1992**, *8*, 429.
(18) Hurter, P.; Hatton, T. A. *Langmuir* **1992**, *8*, 1291. Hurter, P.; Scheutjens, J. M. H. M.; Hatton, T. A. *Macromolecules*, in press.
(19) Böhmer, M. R.; Koopal, L. K.; Lyklema, J. *J. Phys. Chem.* **1991**, *95*, 9569.
(20) Theodorou, D. N. *Macromolecules* **1989**, *22*, 4578.
(21) Napper, D. H. *J. Colloid Interface Sci.* **1977**, *58*, 390. Croucher, M. D.; Hair, M. L. *Macromolecules* **1978**, *11*, 874.
(22) Patel, S. S.; Tirrell, M. In *Annual Review of Physical Chemistry*; Rollefson, G. K., Ed.; Annual Reviews: Palo Alto, CA, 1989; Vol. 40, p 1.
(23) Taunton, H. J.; Toprakcioglu, C.; Fettes, L. J.; Klein, J. *Macromolecules* **1990**, *23*, 571.
(24) Cahn, J. W.; Hilliard, J. E. *J. Chem. Phys.* **1958**, *28*, 258.
(25) Flory, P. *Principles of Polymer Chemistry*; Cornell: Ithaca, NY, 1953.
(26) Sanchez, I. C.; Lacombe, R. H. *J. Phys. Chem.* **1976**, *80*, 2352. Sanchez, I. C.; Lacombe, R. H. *Macromolecules* **1978**, *11*, 1145.
(27) Sanchez, I. C. *Encyclopedia of Physical Science and Technology*; Academic Press: New York, 1987; Vol. XI, p 1.
(28) Cosgrove, T.; Heath, T.; van Lent, B.; Leermakers, F.; Scheutjens, J. *Macromolecules* **1987**, *20*, 1692.
(29) van Lent, B.; Scheutjens, J. M. H. M.; Fleer, G. J. *J. Colloid Interface Sci.* **1990**, *137*, 380.
(30) Peck, D. G. Ph.D. Dissertation, University of Texas, 1992.
(31) Cosgrove, T.; Heath, T. G.; Phipps, J. S.; Richardson, R. M. *Macromolecules* **1991**, *24*, 94.
(32) Fleer, G. J.; Scheutjens, J. M. H. M. *J. Colloid Interface Sci.* **1986**, *111*, 504.
(33) Marra, J.; Hair, M. L. *Colloids Surf.* **1988/1989**, *34*, 215.
(34) Adamson, A. W. *Physical Chemistry of Surfaces*; Wiley: New York, 1990; p 267.